RSC Advances

PAPER

View Article Online
View Journal | View Issue

Cite this: *RSC Adv.*, 2020, **10**, 38369

Self-template formation of porous Co_3O_4 hollow nanoprisms for non-enzymatic glucose sensing in human serum†

Danhua Ge,‡ Yunqi Yang,‡ Xiao Ni, Jinnan Dong, Qianying Qiu, Xue-Qiang Chu and Xiaojun Chen *

Received 24th July 2020
Accepted 8th October 2020

DOI: 10.1039/d0ra06453j

rsc.li/rsc-advances

A novel type of porous Co_3O_4 hollow nanoprism (HNP) was successfully prepared using tetragonal cobalt acetate hydroxide $[Co_5(OH)_2(OAc)_8 \cdot 2H_2O]$ as precursor by a facile solvothermal process and a subsequent calcination treatment. The morphology and structure of the Co_3O_4 HNPs were characterized by scanning electron microscopy (SEM), transmission electron microscopy (TEM), X-ray photoelectron spectroscopy (XPS), powder X-ray diffraction (XRD) and N_2 adsorption–desorption measurements. An enzyme-free glucose sensor was constructed based on the Co_3O_4 HNPs, and the electrochemical performance was tested by cyclic voltammetry (CV) and chronoamperometry. The as-prepared sensor exhibited a good electrocatalytic activity for glucose oxidation at the applied potential of 0.6 V in alkaline solution, with a high sensitivity of 19.83 μA mM^{-1} cm^{-2} and a high upper limit of 30 mM, which provide the potential for direct determination of blood glucose without any dilution pretreatment. The Co_3O_4 HNPs had a porous and tubular structure with a large amount of accessible active sites, which enhanced the mass diffusion and accelerated the electron transfer. Moreover, the sensor also demonstrated a desirable stability, selectivity and reproducibility, and could verify the non-enzymatic analysis of glucose in real samples.

Introduction

The fields of food analysis, clinical diagnostics, fermentation and biotechnology have relied on glucose detection for decades.[1–3] As an essential biological molecule in blood, glucose can provide energy to maintain normal activities.[4] The glucose level in the blood is controlled by a peptide hormone, insulin, and yet, once the insulin secretions are disrupted, human diabetes will be caused.[5] As a result, the precise and rapid determination of glucose concentration is of importance for the healthy development of society and human beings. Various technologies have been applied in glucose detection such as gas chromatography, conductometry, fluorescence based optical methods, mass spectrometry, electrochemistry, calorimetry, *etc.*[6–11] Particularly, electrochemical sensors have drawn attention.[4,12,13] In general, the classic enzymatic glucose biosensors like glucose oxidase (GO_x)-based sensors have been developed for glucose monitoring with high sensitivity and excellent selectivity, but the disadvantages derived from the intrinsic nature of enzymes restrict their practical application.[14] In order to address these problems, massive efforts have been devoted to developing non-enzymatic glucose biosensors with the aid of electrocatalysts, which have the benefits of rapid response speed, good stability, simple fabrication and low cost.

It is well-known that the performance of non-enzymatic glucose biosensors largely depends on the electrocatalysts modified on the electrode surface.[15] Until now, several noble nanomaterials (*e.g.*, Pt, Ag, Pd, Au) and their alloy have been extensively explored as electrocatalysts for electrocatalytic oxidation of glucose with low detection limit.[16–20] Unfortunately, the surfaces of noble metal-based materials are usually easy to be poisoned by adsorbed intermediates and chloride ions, which will result in poor stability and low sensitivity.[21,22] Previous studies demonstrate that transition metal oxides, such as ZnO_x, MnO_x, NiO_x, CuO_x and CoO_x can be employed as ideal materials for the non-enzymatic glucose detection owing to low cost, abundant source, outstanding redox behavior, simple production and stability.[22–27] Among them, Co_3O_4 boasting two oxidation states (Co^{2+} and Co^{3+}), is a magnetic p-type semiconductor and has received considerable attention because of excellent electrocatalytic activity.[28] For instance, Hu *et al.* prepared Co_3O_4 nanoparticles using metal–organic frameworks (MOFs) as template, and then Co_3O_4 nanoparticles were developed as electrode towards glucose detection with low detection limit of 0.13 μM (S/N = 3), high sensitivity of 520.7 mA mM^{-1} cm^{-2} and good selectivity.[29] Choi's group demonstrated that the

College of Chemistry and Molecular Engineering, Nanjing Tech University, Nanjing, 211800, PR China. E-mail: chenxj@njtech.edu.cn

† Electronic supplementary information (ESI) available: The TGA curve, XRD pattern of Co precursor and EDS of the Co_3O_4 HNPs. See DOI: 10.1039/d0ra06453j

‡ D. H. Ge and Y. Q. Yang contributed equally to this work.

porous Co_3O_4@graphene microspheres were constructed by one-step hydrothermal method, which achieved high electrocatalytic performance to direct oxidation of glucose.[22] In spite of these efforts, the rapid and simple preparation of Co_3O_4 nanomaterials is still urgently needed, which can be applied in cost-effective and scalable electrochemical sensors towards glucose determination.

In this study, we reported a simple and scalable synthesis of porous Co_3O_4 HNPs using cobalt acetate hydroxide [$Co_5(OH)_2(OAc)_8 \cdot 2H_2O$] as precursor, followed by the thermal treatment under air atmosphere. The obtained porous Co_3O_4 HNPs exhibited catalytic ability to glucose and thus were employed to fabricate an enzyme-free electrochemical sensor for glucose detection in an alkaline medium. Due to the good stability, selectivity and repeatability, the as-prepared glucose sensor could realize the glucose analysis in real serum samples.

Experimental

Materials

All reagents are analytical reagents, and they were used without further purification. The experimental water was double distilled water. Specifically, cobalt(II) acetate tetrahydrate ($Co(OAc)_2 \cdot 4H_2O$), urea, ethanol, sodium hydroxide (NaOH), D-(+)-glucose, glycine (Gly), L-ascorbic acid (AA), fructose (Fru), uric acid (UA) and L-cysteine (Lcy) were purchased from Additionally, perfluorosulfonic acid (Nafion, 5 wt%) was purchased from DuPont, and diluted to 0.5 wt% for use.

Apparatus

The morphologies and size were characterized by scanning electron microscopy (SEM) (Hitachi S4800) and transmission electron microscopy (TEM) (JEOL JEM-200CX) fitted with energy dispersive X-ray spectroscopy (EDS). The surface elemental oxidation conditions were analyzed by X-ray photoelectron spectroscopy (XPS) (PHI5000 VersaProbe spectrometer, utilizing the Al-Kα X-ray source). The crystalline structure and phase purity were characterized by X-ray diffraction (XRD) (Rigaku Smartlab). The thermogravimetry analysis (TGA) was carried out on TGA 4000 Perkin Elmer Co., Ltd. The nitrogen sorption and desorption isotherms were measured with a Micromeritics ASAP 2020 analyzer. The specific surface area of Co_3O_4 HNPs was determined using the standard Brunauer–Emmett–Teller (BET) method, while the pore size distribution was calculated by the Barrett–Joyner–Halenda (BJH) method.

Preparation of Co_3O_4 HNPs

The porous Co_3O_4 HNPs were synthesized according to an evolution pathway based on a previous literature,[30] which was depicted in Scheme 1. $Co(OAc)_2 \cdot 4H_2O$ and urea with molar ratio of 1 : 6.2 were dissolved into 50 mL of ethanol, and then the solution was heating reflux at 65 °C for 4 h. After completion, the cobalt acetate hydroxide [$Co_5(OH)_2(OAc)_8 \cdot 2H_2O$] precursor of purple NPs were collected by centrifugation and washed with anhydrous ethanol for three times. The product was obtained after drying at 80 °C in air. Afterwards, the freshly-prepared Co precursor was annealed in air for 3 h at 350 °C with a heating rate of 1 °C min^{-1}. After the thermal treatment, the color of the product changed from purple to black, and thus the porous Co_3O_4 HNPs were obtained.

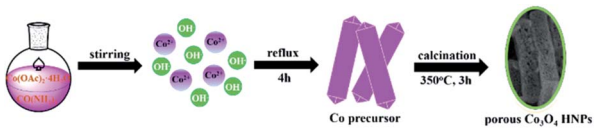

Scheme 1 Schematics of the Co_3O_4 HNPs morphology evolution.

Electrochemical measurements

Cyclic voltammogram (CV) and chronoamperometry were performed with a CHI 660D electrochemical workstation (Chenhua Instrument Co., Shanghai, China). All experiments were performed using a three-electrode electrochemical system with a modified ITO working electrode (Φ = 3 mm), a saturated calomel reference electrode (SCE) and a platinum slice counter electrode. All ITO electrodes were washed successively by acetone, ethanol and water before use. After drying with nitrogen, 10 μL of 1 mg mL^{-1} Co_3O_4 HNPs dispersion in 0.5 wt% of Nafion was casted onto ITO electrode and then let it dry in air at room temperature. The detection of glucose was carried out in 0.05 M NaOH, and the current response of the sensor was the subtraction of total current and the background ($\Delta I = I_p - I_0$).

Results and discussion

Characterization of Co precursor

The morphology and structure of Co precursor were characterized by SEM and TEM, which were shown in Fig. 1. It could be

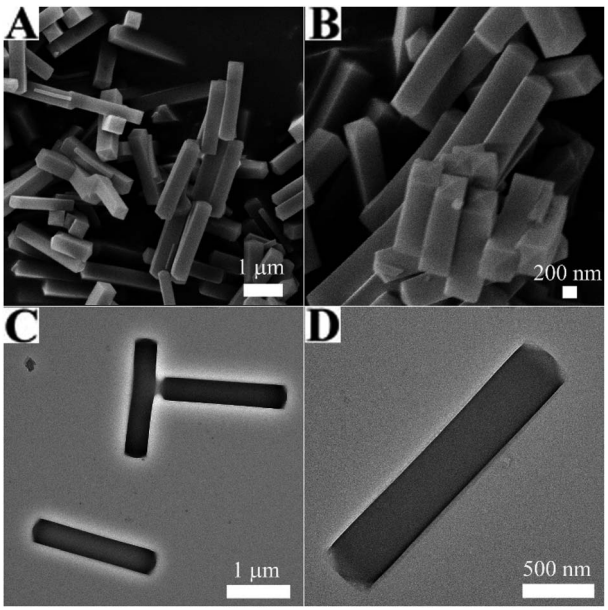

Fig. 1 (A and B) SEM and (C and D) TEM images of Co precursor.

found from Fig. 1A and B that the morphology of Co precursor is a uniform NP with smooth outer surface, and the length was ~2 μm and the diameter was ~380 nm. Observed from the corresponding TEM images (Fig. 1C and D), the Co precursor was solid. Fig. S1† displayed the TGA curve of the Co precursor under air atmosphere. It could be seen the first slight weight loss between 10–250 °C, resulting from the removal of adsorbed water and ethanol. The subsequently obvious and sharp weight loss between 250-300 °C might correspond to the complete decomposition of Co precursor to Co_3O_4. Therefore, in order to ensure that the burning is complete and the morphology remains unchanged, the optimal annealing condition of Co precursor is 350 °C in air. In addition, the XRD pattern of Co precursor was in full agreement with the tetragonal $Co_5(OH)_2(OAc)_8 \cdot 2H_2O$ phase (JCPDS Card No. 22-0582) shown in Fig. S2,†[31] which was prepared as the self-engaged template.

Characterization of the Co_3O_4 HNPs

After calcination, the Co_3O_4 HNPs were achieved. Compared with the Co precursor, the SEM images of the Co_3O_4 HNPs in Fig. 2A and B exhibited the similar size and shape, but porous structure was formed. More structure information are revealed by TEM, as seen in Fig. 2C and D. The Co_3O_4 HNPs have large central void space and the grained shell with the thickness of ~40 nm, owing to the release of CO_2 and water during the calcination process. Furthermore, EDS (figure determined the chemical composition of Co_3O_4 sample S3) and the strong Co and O peak signals were found (other peaks originated from the ITO substrate). To further clarify the crystalline structure of the Co_3O_4 HNPs, the HRTEM in Fig. 2E identified two well-defined lattice fringes of 0.47 and 0.26 nm, which are attributed to the (111) and (311) lattice plane of the Co_3O_4 phase, respectively, according to the calculation of Bragg's equation ($2d \sin\theta = n\lambda$).[31] The powder XRD pattern of Co_3O_4 HNPs (Fig. 2F) shown the diffraction peaks at 19.3°, 31.5°, 36.9°, 44.9°, 55.8°, 59.5° and 65.5° (2θ), which were designated to the (111), (220), (311), (400), (422), (511) and (440) crystal planes of the spinel-type Co_3O_4 (JCPDS Card No. 43-1003).[32] In addition, it can be observed from the XRD analysis with no other impurity phases, which indicates that the Co precursor was completely converted into Co_3O_4 HNPs after calcination treatment.

To confirm the valence states and corresponding element information of the Co_3O_4 HNPs, the detailed XPS measurements were performed. Fig. 3A showed the presence of Co and O elements in the XPS survey spectrum of Co_3O_4 HNPs. In Fig. 3B, the regional Co 2p spectrum exhibited two contributions located at 794.7 eV and 779.7 eV, which correspond to $2p_{1/2}$ and $2p_{3/2}$, respectively. In particular, the two peaks located at 774.6 and 779.6 eV were assigned to the $2p_{1/2}$ and $2p_{3/2}$ of Co^{3+}, while peaks at 796.1 and 780.9 eV signify the $2p_{1/2}$ and $2p_{3/2}$ of Co^{2+}, respectively, confirming the product of Co_3O_4 species.[33] Moreover, the two small peaks located around 789.5 and 804.4 eV correspond to Co^{2+} shake-up satellite peaks, which further verify the formation of Co_3O_4 crystal phase. From the XPS O 1s spectrum in Fig. 3C, the peaks at about 529.8 and 531.3 eV are ascribed to lattice oxygen and hydroxyl group, respectively.[34] Afterwards, the specific surface area and porous feature of the Co_3O_4 HNPs were measured by N_2 adsorption–desorption isotherms at 77 K. It is well known that most of physisorption

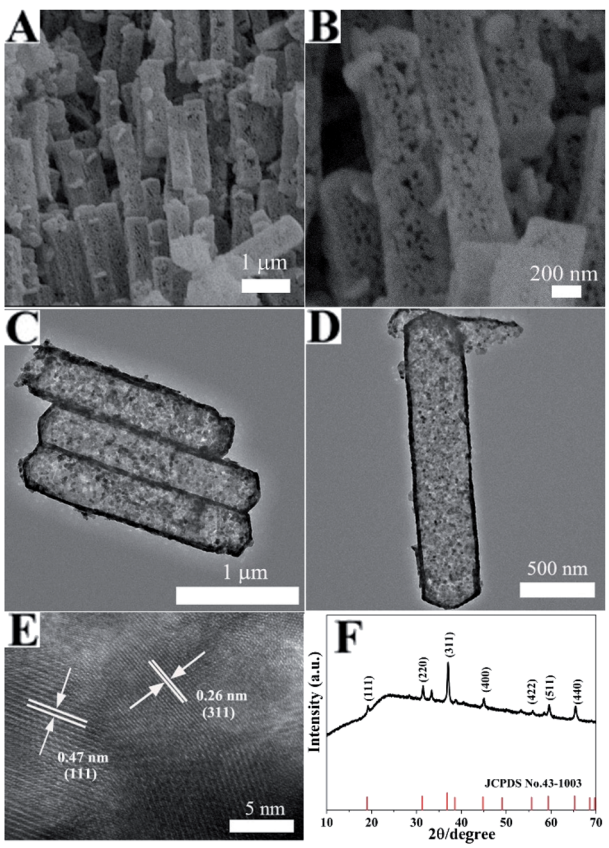

Fig. 2 (A and B) SEM, (C and D) TEM and (E) HRTEM images of the Co_3O_4 HNPs, (F) XRD pattern of the Co_3O_4 HNPs.

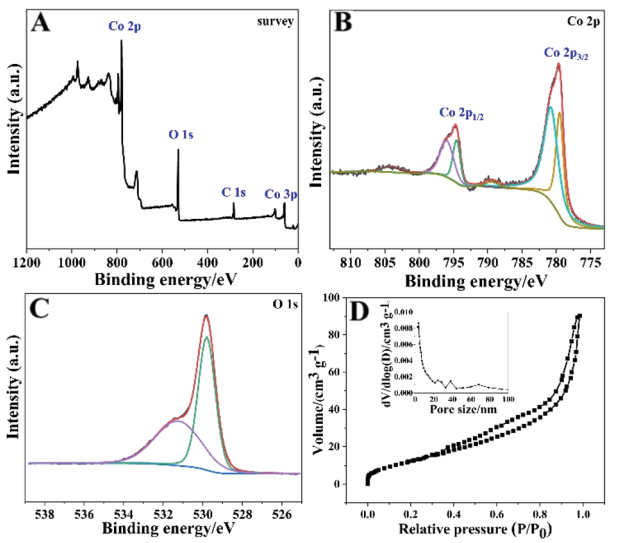

Fig. 3 (A) XPS survey spectrum of the Co_3O_4 HNPs, and high-resolution XPS spectra of (B) Co 2p and (C) O 1s. (D) N_2 adsorption–desorption isotherm of the Co_3O_4 HNPs. Inset: the pore size distribution curve.

isotherms can be divided into six types based on the Brunauer–Deming–Deming–Teller (BDDT) classification.[35] As presented in Fig. 3D, the Co_3O_4 HNPs display an isotherm of Type IV with a distinct hysteresis loop of H3 due to the presence of mesoporous structure.[36] The calculated BET specific surface area was determined as about 50.8 $m^2\ g^{-1}$ by the BET analysis. Besides, the pore size distribution curve of the sample (Fig. 3D, inset) displayed peaks at 3.7 nm, 24.5 nm and 38.3 nm belonging to mesopores by the BJH analysis, demonstrating the pyrolysis of Co precursor.[37] Such structural features of the large specific surface area and porosity can allow Co_3O_4 HNPs to expose more active sites for efficient mass transport of ions and electrons between the electrode and electrolyte interface, thereby elevating the electrochemical property.

Electrochemical catalysis of Co_3O_4 HNPs towards glucose

Initially, the electrochemical behaviors of the Co_3O_4 HNPs and bare ITO towards glucose oxidation were characterized by CVs in the potential range of 0.2–0.65 V. Fig. 4A presented the CV curves of the Co_3O_4 HNPs modified electrode in the absence (curve *a*) and presence (curve *b*) of 1 mM glucose in 0.1 M NaOH electrolyte at a scan rate of 50 mV s^{-1}, and two pairs of redox peaks can be observed with anodic peaks at around 0.52 V and 0.3 V and cathodic peaks at around 0.44 V and 0.23 V, respectively, which indicated that electroactive substance existed on the surface of ITO. When glucose was added into NaOH, the electrocatalytic activity of Co_3O_4 HNPs toward glucose oxidation was confirmed by the increasing the anodic peak and the decreasing of cathodic peak.[38] Here, one pair of poorly defined redox peaks were located at 0.3 V and 0.23 V for the transfer between Co_3O_4 and CoOOH, whereas the other pair of well-defined peaks appeared at 0.52 V and 0.44 V corresponding to the reversible transition between CoOOH and CoO_2. The remarkable current increase in the presence of glucose may suggest that the oxidation of glucose to gluconolactone at the as-prepared Co_3O_4 HNPs is mainly electrocatalyzed by CoOOH/CoO_2 redox couple rather than Co_3O_4/CoOOH in NaOH solution. And the corresponding equations were described as follows:[29,32]

$$Co_3O_4 + OH^- + H_2O \leftrightarrow 3CoOOH + e^- \quad (1)$$

$$CoOOH + OH^- \leftrightarrow CoO_2 + H_2O + e^- \quad (2)$$

$$2CoO_2 + C_6H_{12}O_6(\text{glucose}) \leftrightarrow 2CoOOH + C_6H_{10}O_6(\text{gluconolactone}) \quad (3)$$

As shown in Fig. 4B, the oxidation peak current increased continuously along with the glucose concentration increased from 0 to 20 mM, demonstrating a good electrochemical catalytic ability towards glucose oxidation. In order to further explore the electrochemical kinetics of Co_3O_4 HNPs, the relationship between the peak current and scan rate was also investigated in the range of 10–150 mV s^{-1}. In Fig. 4C, it was found that the current increased with increasing the scan rate, and both the oxidation and reduction peak currents (I_{pa} and I_{pc}) were in proportion to the square root of the scan rate ($v^{1/2}$) with the correlation coefficients R^2 of 0.9823 (I_{pa}) and 0.9910 (I_{pc}), respectively (Fig. 4D). The presented typically diffusion-controlled electrochemical behavior illustrated the fast electron transfer between electrode surface and Co_3O_4 HNPs modification. It was might attributed to the porous and hollow structure of Co_3O_4 HNPs, which provided more pathways for electron transfer and thus accelerate the electron transfer rate.

Experimental parameters optimization

The alkaline electrolyte is beneficial to improve the electrochemical catalytic activity of the Co_3O_4 HNPs in non-enzymatic glucose sensors,[22,39] so the influence of NaOH concentration need to be investigated. The CV curves recorded in NaOH solution with different concentrations (0.001–0.5 M) containing 1 mM glucose between 0.0 V and 0.7 V at 50 mV s^{-1} were shown in Fig. 5A. The oxidative peak current rose correspondingly

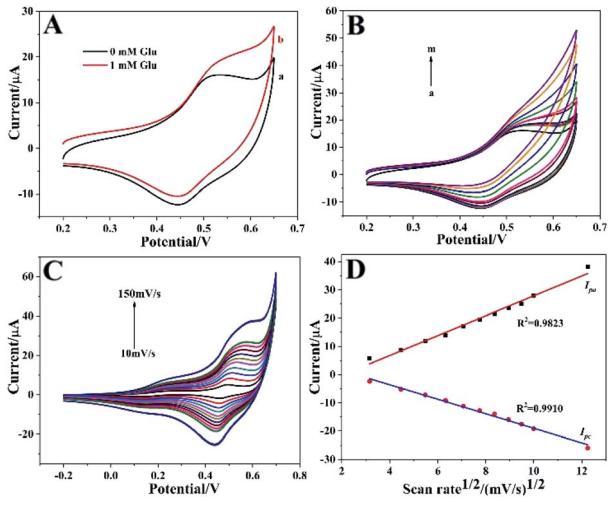

Fig. 4 (A) CVs of Co_3O_4 HNPs/ITO in the absence (a) and presence (b) of 1 mM glucose. Scan rate: 50 mV s^{-1}. (B) CV curves of Co_3O_4 HNPs/ITO recorded towards different concentrations of glucose (from a to m: 0, 0.01, 0.02, 0.05, 0.1, 0.2, 0.5, 1, 2, 5, 10, 15 and 20 mM, respectively). (C) CVs of Co_3O_4 HNPs/ITO in 0.1 M NaOH at different scan rate from 10 to 150 mV s^{-1}. (D) The calibration plots of I_{pa} (a) and I_{pc} (b) *vs.* $v^{1/2}$.

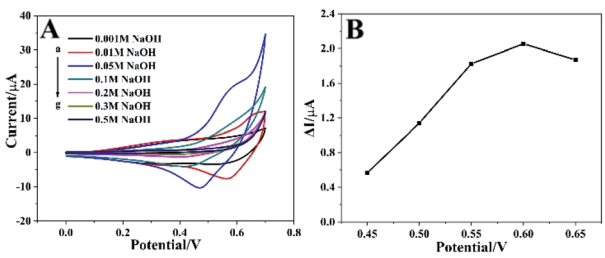

Fig. 5 (A) CVs of Co_3O_4 HNPs/ITO recorded in N_2 saturated NaOH solution with different concentrations containing 1 mM glucose (from a to g: 0.001, 0.01, 0.05, 0.1, 0.2, 0.3, 0.5 M, respectively). (B) Effect of applied potential on the amperometric response of Co_3O_4 HNPs/ITO in N_2 saturated 0.05 M NaOH solution containing 1 mM glucose. Scan rate is 50 mV s^{-1}.

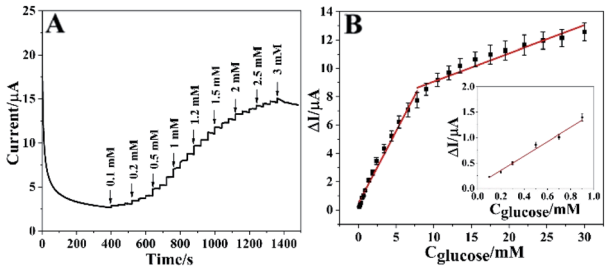

Fig. 6 (A) Chronoamperometric curve of Co_3O_4 HNPs towards glucose with successive addition in 0.05 M NaOH at the working potential of 0.6 V. (B) The calibration curve of the glucose sensor. Inset: high magnification linear range for 0.1 to 0.9 mM of glucose concentration.

when NaOH concentration increased from 0.001 to 0.05 M, owing to the increasing availability of hydroxyl ion (OH^-) and improved electrocatalytic activity of Co_3O_4 HNPs on the glucose oxidation. Nevertheless, the oxidative peak current decreased when the NaOH concentration exceeded 0.05 M, and the reason might be that too much OH- ion covered the surface of catalyst so that the adsorption of glucose was hindered, which caused a decreased current signal.[39,40] Therefore, the electrolyte concentration was an important element in the electrochemical reaction and OH^- also played a role in the catalysis process. As a result, the optimal NaOH solution was chosen as 0.05 M for our proposed Co_3O_4 HNPs-based non-enzymatic glucose sensor.

The effect of applied potential on the steady-state current response was also studied. As presented in Fig. 5B, the amperometric current response ΔI was found increased rapidly with the potential positively shifted from 0.45 to 0.6 V, and decreased at 0.65 V. Significantly, the higher working potential usually generates serious interference and larger background noise.[38] Therefore, 0.6 V was chosen as the optimum working potential to investigate the performance of the Co_3O_4 HNPs towards the oxidation of glucose.

Quantitative detection of glucose

Under the optimal conditions, the real-time electrocatalytic response of different amount of glucose on Co_3O_4 HNPs/ITO was performed using chronoamperometry technique at an applied potential of 0.6 V. In Fig. 6A, a rapid current increment could be observed along with the glucose concentration increased from 0.1 to 30 mM. When the glucose concentration exceeded 30 mM, the current response became gradually decreased, probably due to the adsorption and diffusion dominance of highly concentrated intermediates onto the active sites of Co_3O_4 HNPs catalyst to impede incoming glucose.[39–42] In addition, the steady-state current response was achieved in about 0.1 s (Fig. S8†), which is much faster than the previous glucose sensors based on metal oxide catalysts.[5,26] It is attributed to the excellent catalytic capability of Co_3O_4 HNPs in alkaline solution, along with the tubular structure facilitating the electron transfer between glucose and electrode surface. Fig. 6B described the corresponding calibration curves involved in the concentration of glucose and the current response, which presented two linear concentration ranges with 0.1–7.8 mM ($R^2 = 0.98$) and 7.8–30 mM ($R^2 = 0.92$), with the linear equations of $\Delta I/\mu A = 1.018 C_{glucose}/mM + 0.464$ and $\Delta I/\mu A = 0.199 C_{glucose}/mM + 7.08$, respectively. The different concentrations of glucose can give rise to the different diffusion rates on catalyst, which produced two linear ranges. And the oxidation products can rapidly detach from the surface of electrode under low concentration of glucose, while the high concentration of glucose hinder the diffusion of the gluconolactone.[34] In consequence, the high concentration of glucose easily leads to lower oxidation peak current and the low concentration range is often accompanied by relatively higher oxidation current.

Then the Co_3O_4 HNPs can manifest a good linearity even at low concentrations in the range from 0.1 to 0.9 mM ($R^2 = 0.99$) with the linear equation of $\Delta I/\mu A = 1.408 C_{glucose}/mM + 0.074$, where 1.408 was the slope (Fig. 6B, inset). Sensitivity is calculated as the result of slope divided by the geometric area of ITO electrode. The geometric area is 0.071 cm^2 since the diameter of ITO working electrode is 3 mm.[43] On the basis of quantitative determination, the sensitivity of the Co_3O_4 HNPs toward glucose oxidation is 19.83 μA mM^{-1} cm^{-2}. Additionally, the limit of detection (LOD) of around 0.0286 mM (S/N = 3) was calculated for glucose at the Co_3O_4 HNPs electrode. It essentially indicates high sensitivity of Co_3O_4 HNPs towards glucose catalysis with a good linear dependence.[26,44] Compared with some previous reports shown in Table 1, it was worth

Table 1 The performance comparison of metal oxide-based electrochemical glucose sensors

Electrode	Linear range/mM	LOD/μM	Sensitivity/μA mM^{-1} cm^{-2}	Ref.
$NiO–SnO_2$	0.01–26	1.0	14	25
Co_3O_4–NiO	0.001–3.4	0.81	62	34
	3.4–12.2			
Co_3O_4/GO	0.09–6.03	0.52	20.1	45
Co_3O_4@MCF-Chi-GOx	0–1.7	107.7	—	46
Co_3O_4 UHMSA	0.1–5	1.84	102.8	47
Co_3O_4 NF/GOH	0.25–10	—	492.8	48
CuO	—	1	5342.8	26
NiO-SDHCNSs	Up to 13	0.052	1697	39
Au@Cu_2O	0.05–2	—	715	15
Co_3O_4 HNPs	0.1–30	28.6	19.83	This work

mentioning that the proposed glucose sensor exhibited a comparatively wider linearity range and a lower detection limit. And the proposed Co_3O_4 HNPs could be directly employed in the real sample analysis due to the wide linear concentration range, which could cover the normal human blood glucose concentration ranges.[5]

Repeatability, reproducibility and selectivity of the glucose sensor

The long-term stability is a very important character for glucose sensing. As illustrated in Fig. 7A, the stability of the sensor was tested by periodically detecting the current responses to 0.5 mM glucose, and the results revealed that the current remained about 95.3% of its initial value even after the sensor was preserved for 25 days at room temperature. It might be due to the inherent good stability of the Co_3O_4 HNPs. In addition, the reproducibility of the constructed glucose sensor was further evaluated. The obtained relative standard deviation (RSD) for different concentrations of glucose were investigated as 5.3%, 4.1% and 2.4%, respectively ($n = 5$), demonstrating its good reproducibility.

As is known, one of the major challenges in non-enzymatic electrochemical sensor is to discern the target molecule from interferents in a complex biological environment.[41] Normally in real human blood serum samples, some co-existed species such as UA, dopamine, AA and other carbohydrate compounds may interfere with the glucose sensing. Thus, in the anti-interference evaluation experiment, 0.34 mM of glucose, UA, AA, Fru, Gly and Lcy were successively added into the system to detect the current response. As shown in Fig. 7B, an obvious current increase appeared when adding glucose, and a minor increase or even a decrease was observed in current response along with the addition of Gly and Fru. In consideration of the physiological level of the glucose concentration is in the range of 4–7 mM, the endogenous interferents are 30 times lower than that of glucose concentration, for example, the concentrations of AA and UA are about 0.125 and 0.33 mM in human blood, respectively.[49–51] Thereinto, Lcy and AA might result in about 1.3% and 1.1% enhancement in current response compared with that from glucose, which can be considered insignificant and negligible.[50] Furthermore, another current increase was obviously observed with a second injection of glucose, which

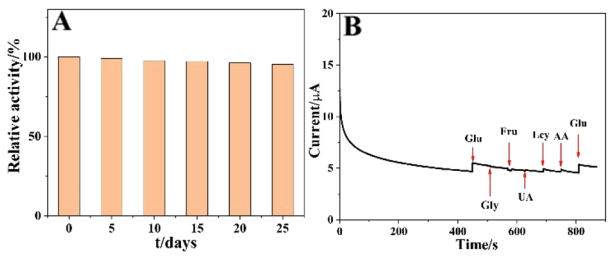

Fig. 7 (A) Relative current responses of the glucose sensor to 0.5 mM glucose during a period of 25 days. (B) Amperometric i–t response on successive addition of 0.34 mM glucose (Glu), Gly, Fru, UA, Lcy, AA and a second addition of glucose (Glu).

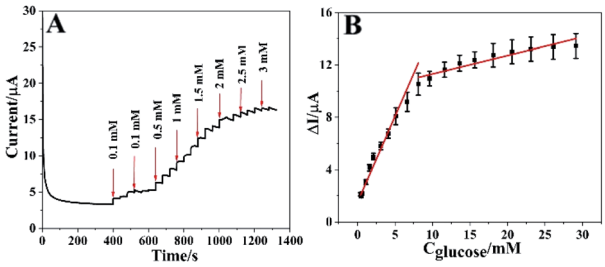

Fig. 8 (A) Chronoamperometric curve of Co_3O_4 HNPs towards glucose with successive addition in 0.05 M NaOH in healthy human serum sample at 0.6 V. (B) The calibration curve of the glucose sensor.

well suggested the excellent anti-interference capability of the glucose sensor.

Real sample application

In order to evaluate the feasibility for practical sample testing, the Co_3O_4-based sensor was employed to detect glucose in healthy human serum sample without pretreatment, which was donated by one volunteer. Fig. 8A displayed the amperometric responses of the glucose sensor in the stirring NaOH solution mixed with 5% human serum. Actually, the first 0.1 mM glucose was injected into 9.5 mL of NaOH, and then 0.5 mL serum was added into it. After mixing thoroughly, a second injection of 0.1 mM glucose was added. Thus, a smaller current response compared with the first injection was observed, owing to the slight interference in real system. After that, the current increased along with the addition of glucose. As illustrated in Fig. 8B, the corresponding calibration curves presented two linear concentration ranges of 0.42–8.1 mM ($R^2 = 0.96$) and 8.1–30 mM ($R^2 = 0.89$), with the linear equations of $\Delta I/\mu A = 1.31C_{glucose}/mM + 1.496$ and $\Delta I/\mu A = 0.14C_{glucose}/mM + 9.901$, respectively. The linearity was consistent with that in Fig. 6, demonstrating a promising future of the developed glucose sensor in practical determination.[49]

Conclusions

In summary, we have successfully developed a simple and scalable synthetic method of Co_3O_4 HNPs by self-template process and calcination treatment, which was immobilized on ITO to fabricate a non-enzymatic glucose sensor. The as-prepared Co_3O_4 HNPs present favourable electrocatalytic capability towards glucose oxidation in alkaline medium with a wide linear range, a low detection limit, a high selectivity and specificity. The results exhibit a scalable, low-cost and effective alternate for developing novel non-enzymatic glucose sensors based on transition metal oxides *via* ingenious structure design.

Ethical statement

The serum sample used in this work was donated by a healthy person, and the informed consent was also obtained from her. All experiments were performed in accordance with the guideline "NJTECH 2019-6", and approved by the Department of

Scientific Research at Nanjing Tech University. Study participants were fully informed regarding the purposes of the study and consent was obtained.

Conflicts of interest

There are no conflicts to declare.

Acknowledgements

This work was financially supported by the National Natural Science Foundation of China (No. 21575064), and the Six Talent Peaks Project in Jiangsu Province (2016-SWYY-022). This work is also sponsored by Qing Lan Project of Education Department of Jiangsu Province.

Notes and references

1 J. He, Y. Zhong, Q. Xu, H. Sun, W. Zhou and Z. Shao, Nitrogen-doped graphic carbon protected Cu/Co/CoO nanoparticles for ultrasensitive and stable non-enzymatic determination of glucose and fructose in wine, *J. Electrochem. Soc.*, 2018, **165**, B543–B550.

2 J. Huang, X. L. Zhu, Y. M. Wang, J. H. Ge, J. W. Liu and J. H. Jiang, A multiplex paper-based nanobiocatalytic system for simultaneous determination of glucose and uric acid in whole blood, *Analyst*, 2018, **143**, 4422–4428.

3 Y. Ma, Y. Mao, Y. An, T. Tian, H. Zhang, J. Yan, Z. Zhu and C. J. Yang, Target-responsive DNA hydrogel for nonenzymatic and visual detection of glucose, *Analyst*, 2018, **143**, 1679–1684.

4 X. R. Chen, D. Liu, G. J. Cao, Y. Tang and C. Wu, In situ synthesis of a sandwich-like graphene@ZIF-67 heterostructure for highly sensitive nonenzymatic glucose sensing in human serums, *ACS Appl. Mater. Interfaces*, 2019, **11**, 9374–9384.

5 N. Karikalan, M. Velmurugan, S. M. Chen and C. Karuppiah, Modern approach to the synthesis of $Ni(OH)_2$ decorated sulfur doped carbon nanoparticles for the nonenzymatic glucose sensor, *ACS Appl. Mater. Interfaces*, 2016, **8**, 22545–22553.

6 W. Q. Xie, Y. X. Gong and K. X. Yu, Rapid quantitative detection of glucose content in glucose injection by reaction headspace gas chromatography, *J. Chromatogr. A*, 2017, **1520**, 143–146.

7 A. A. Shulga, A. P. Soldatkin, A. V. Elskaya, S. V. Dzyadevich, S. V. Patskovsky and V. I. Strikha, Thin-film conductometric biosensors for glucose and urea determination, *Biosens. Bioelectron.*, 1994, **9**, 217–223.

8 J. C. Pickup, F. Hussain, N. D. Evans, O. J. Rolinski and D. J. S. Birch, Fluorescence-based glucose sensors, *Biosens. Bioelectron.*, 2005, **20**, 2555–2565.

9 C. W. Tsao and Z. J. Yang, High sensitivity and high detection specificity of gold-nanoparticle-grafted nanostructured silicon mass spectrometry for glucose analysis, *ACS Appl. Mater. Interfaces*, 2015, **7**, 22630–22637.

10 N. Daisuke, T. Yukikazu, W. Masayoshi and K. Kazunori, Simple and precise preparation of a porous gel for a colorimetric glucose sensor by a templating technique, *Angew. Chem., Int. Ed.*, 2003, **115**, 4329–4332.

11 N. S. Oliver, C. Toumazou, A. E. G. Cass and D. G. Johnston, Glucose sensors: a review of current and emerging technology, *Diabet. Med.*, 2009, **26**, 197–210.

12 N. I. Chandrasekaran and M. Matheswaran, A sensitive and selective non-enzymatic glucose sensor with hollow Ni-AlMn layered triple hydroxide nanocomposites modified Ni foam, *Sens. Actuators, B*, 2019, **288**, 188–194.

13 J. N. Xu, F. H. Li, D. D. Wang, M. H. Nawaz, Q. B. An, D. X. Han and L. Niu, Co_3O_4 nanostructures on flexible carbon cloth for crystal plane effect of nonenzymatic electrocatalysis for glucose, *Biosens. Bioelectron.*, 2019, **123**, 25–29.

14 G. Sparacino, M. Zanon, A. Facchinetti, C. Zecchin, A. Maran and C. Cobelli, Italian contributions to the development of continuous glucose monitoring sensors for diabetes management, *Sensors*, 2012, **12**, 13753–13780.

15 Y. Su, H. Guo, Z. S. Wang, Y. M. Long, W. F. Li and Y. F. Tu, $Au@Cu_2O$ core-shell structure for high sensitive non-enzymatic glucose sensor, *Sens. Actuators, B*, 2018, **255**, 2510–2519.

16 S. Park, T. D. Chung and H. C. Kim, Nonenzymatic glucose detection using mesoporous platinum, *Anal. Chem.*, 2003, **75**, 3046–3049.

17 M. Baghayeri, A. Amiri and S. Farhadi, Development of non-enzymatic glucose sensor based on efficient loading Ag nanoparticles on functionalized carbon nanotubes, *Sens. Actuators, B*, 2016, **225**, 354–362.

18 X.-M. Chen, Z.-J. Lin, D.-J. Chen, T.-T. Jia, Z.-M. Cai, X.-R. Wang, X. Chen, G.-N. Chen and M. Oyama, Nonenzymatic amperometric sensing of glucose by using palladium nanoparticles supported on functional carbon nanotubes, *Biosens. Bioelectron.*, 2010, **25**, 1803–1808.

19 Y. Fan, X. Tan, X. Ou, S. Chen and S. Wei, An ultrasensitive electrochemiluminescence biosensor for the detection of concanavalin a based on Au nanoparticles-thiosemicarbazide functionalized PtNi nanocubes as signal enhancer, *Biosens. Bioelectron.*, 2017, **87**, 802–806.

20 C. Zhang, Y. Zhang, X. Du, Y. Chen, W. Dong, B. Han and Q. Chen, Facile fabrication of Pt-Ag bimetallic nanoparticles decorated reduced graphene oxide for highly sensitive non-enzymatic hydrogen peroxide sensing, *Talanta*, 2016, **159**, 280–286.

21 K. E. Toghill and R. G. Compton, Electrochemical non-enzymatic glucose sensors: a perspective and an evaluation, *Int. J. Electrochem. Sci.*, 2010, **5**, 1246–1301.

22 M. H. Yang, J.-M. Jeong, K. G. Lee, D. H. Kim, S. J. Lee and B. G. Choi, Hierarchical porous microspheres of the Co_3O_4@graphene with enhanced electrocatalytic performance for electrochemical biosensors, *Biosens. Bioelectron.*, 2017, **89**, 612–619.

23 W. Raza and K. Ahmad, A highly selective Fe@ZnO modified disposable screen printed electrode based non-enzymatic

glucose sensor (SPE/Fe@ZnO), *Mater. Lett.*, 2018, **212**, 231–234.

24 L. Han, J. Shi and A. Liu, Novel biotemplated MnO_2 1D nanozyme with controllable peroxidase-like activity and unique catalytic mechanism and its application for glucose sensing, *Sens. Actuators, B*, 2017, **252**, 919–926.

25 Y. Zhou, X. Ni, Z. Ren, J. Y. Ma, J. Z. Xu and X. J. Chen, A flower-like NiO-SnO_2 nanocomposite and its non-enzymatic catalysis of glucose, *RSC Adv.*, 2017, **7**, 45177–45184.

26 S. K. Meher and G. R. Rao, Archetypal sandwich-structured CuO for high performance non-enzymatic sensing of glucose, *Nanoscale*, 2013, **5**, 2089–2099.

27 B. Wang, Y. F. Cheng, H. Su, M. Cheng, Y. Li, H. B. Geng and Z. F. Dai, *Boosting transport kinetics of cobalt sulfides yolk–shell spheres by anion doping for advanced lithium and sodium storage*, 2020, DOI: 10.1002/cssc.202001261.

28 J. Yu, Y. H. Ni and M. H. Zhai, Highly selective non-enzyme glucose detection based on Co-CoO-Co_3O_4 nanocomposites prepared *via* a solution-combustion and subsequent heat-treating route, *J. Alloys Compd.*, 2017, **723**, 904–911.

29 C. T. Hou, Q. Xu, L. N. Yin and X. Y. Hu, Metal-organic framework templated synthesis of Co_3O_4 nanoparticles for direct glucose and H_2O_2 detection, *Analyst*, 2012, **137**, 5803–5808.

30 S. Asuha, S. Zhao, H. Y. Wu, L. Song and O. Tegus, One step synthesis of maghemite nanoparticles by direct thermal decomposition of Fe–urea complex and their properties, *J. Alloys Compd.*, 2009, **472**, L23–L25.

31 L. Yu, J. F. Yang and X. W. D. Lou, Formation of CoS_2 nanobubble hollow prisms for highly reversible lithium storage, *Angew. Chem., Int. Ed.*, 2016, **55**, 13422–13426.

32 E. H. Zhang, Y. Xie, S. Q. Ci, J. C. Jia and Z. H. Wen, Porous Co_3O_4 hollow nanododecahedra for nonenzymatic glucose biosensor and biofuel cell, *Biosens. Bioelectron.*, 2016, **81**, 46–53.

33 D. H. Ge, H. B. Geng, J. Q. Wang, J. W. Zheng, Y. Pan, X. Q. Cao and H. W. Gu, Porous nano-structured Co_3O_4 anode materials generated from coordination-driven self-assembled aggregates for advanced lithium ion batteries, *Nanoscale*, 2014, **6**, 9689–9694.

34 Y. J. Gao, Q. H. Yua, Y. T. Du, M. Yang, L. Gao, S. Q. Rao, Z. Q. Yang, Q. C. Lan and Z. J. Yang, Synthesis of Co_3O_4-NiO nano-needles for amperometric sensing of glucose, *J. Electroanal. Chem.*, 2019, **838**, 41–47.

35 Q. Li, B. D. Guo, J. G. Yu, J. R. Ran, B. H. Zhang, H. J. Yan and J. R. Gong, Highly efficient visible-light-driven photocatalytic hydrogen production of CdS-cluster-decorated graphene nanosheets, *J. Am. Chem. Soc.*, 2011, **133**, 10878–10884.

36 K. S. W. Sing, D. H. Everett, R. Haul, L. Moscou, R. A. Pierotti, J. Rouquerol and T. Siemieniewska, Reporting physisorption data for gas/solid systems with special reference to the determination of surface area and porosity, *Pure Appl. Chem.*, 1985, **57**, 603–619.

37 S. G. Kim, J. Jun, Y. K. Kim, J. Kim, J. S. Lee and J. Jang, Facile synthesis of Co_3O_4-incorporated multichannel carbon nanofibers for electrochemical applications, *ACS Appl. Mater. Interfaces*, 2020, **12**, 20613–20622.

38 Z. Y. Yang, X. Bai, C. C. Qi and J. M. You, Shape-controlled synthesis of sulfur-doped Co_3O_4 for enhanced nonenzymatic detection of glucose, *J. Electrochem. Soc.*, 2020, **167**, 027518.

39 R. Madhuvilakku, R. Mariappan, S. Alagar and S. Piraman, Sensitive and selective non-enzymatic detection of glucose by monodispersed NiO@S-doped hollow carbon sphere hybrid nanostructures, *Anal. Chim. Acta*, 2018, **1042**, 93–108.

40 X. Zhang, Y. D. Xu and B. X. Ye, An efficient electrochemical glucose sensor based on porous nickel-based metal organic framework/carbon nanotubes composite (NiMOF/CNTs), *J. Alloys Compd.*, 2018, **767**, 651–656.

41 G. H. Wu, X. H. Song, Y. F. Wu, X. M. Chen, F. Luo and X. Chen, Non-enzymatic electrochemical glucose sensor based on platinum nanoflowers supported on graphene oxide, *Talanta*, 2013, **105**, 379–385.

42 K. K. Naik, A. Gangan, B. Chakraborty, S. K. Nayak and C. S. Rout, Enhanced nonenzymatic glucose-sensing properties of electrodeposited $NiCo_2O_4$-Pd nanosheet: experimental and DFT investigations, *ACS Appl. Mater. Interfaces*, 2017, **9**, 23894–23903.

43 S. R. Balakrishnan, U. Hashim, G. R. Letchumanan, M. Kashif, A. R. Ruslinda, W. W. Liu, P. Veeradasan, R. Haarindra Prasad, K. L. Foo and P. Poopalan, Development of highly sensitive polysilicon nanogap with APTES/GOx based lab on chip biosensor to determine low levels of salivary glucose, *Sens. Actuators, A*, 2014, **220**, 101–111.

44 X. Xiao, S. S. Zheng, X. R. Li, G. X. Zhang, X. T. Guo, H. G. Xue and H. Pang, Facile synthesis of ultrathin Ni-MOF nanobelts for high-efficiency determination of glucose in human serum, *J. Mater. Chem. B*, 2017, **5**, 5234–5239.

45 G. P. Dai, P. Lu, Y. Liang and Y. T. Lei, Preparation of Co_3O_4/graphene oxide composites by a depositing-decompostion method and its application for electrochemical determination of glucose, *J. Chin. Chem. Soc.*, 2013, **60**, 366–370.

46 Dhanjai, P. Balla, A. Sinha, L. X. Wu, X. B. Lu, D. Q. Tan and J. P. Chen, Co_3O_4 nanoparticles supported mesoporous carbon framework interface for glucose biosensing, *Talanta*, 2019, **203**, 112–121.

47 L. J. Ding, M. G. Zhao, S. S. Fan, Y. Ma, J. J. Liang, X. T. Wang, Y. W. Song and S. G. Chen, Preparing Co_3O_4 urchin-like hollow microspheres self-supporting architecture for improved glucose biosensing performance, *Sens. Actuators, B*, 2016, **235**, 162–169.

48 L. T. Hoa, J. S. Chung and S. H. Hur, A highly sensitive enzyme-free glucose sensor based on Co_3O_4 nanoflowers and 3D graphene oxide hydrogel fabricated *via* hydrothermal synthesis, *Sens. Actuators, B*, 2016, **223**, 76–82.

49 Q. Z. Zhu, S. Y. Hu, L. Q. Zhang, Y. Li, C. Carraro, R. Maboudian, W. Wei, A. R. Liu, Y. J. Zhang and S. Q. Liu, Reconstructing hydrophobic ZIF-8 crystal into hydrophilic hierarchicallyporous nanoflowers as catalyst carrier for

nonenzymatic glucose sensing, *Sens. Actuators, B*, 2020, **313**, 128031.

50 L. Sinha, S. Pakhira, P. Bhojane, S. Mali, C. K. Hong and P. M. Shirage, Hybridization of Co_3O_4 and α-MnO_2 nanostructures for high-performance nonenzymatic glucose sensing, *ACS Sustainable Chem. Eng.*, 2018, **6**, 13248–13261.

51 R. M. Abdel Hameed, Amperometric glucose sensor based on nickel nanoparticles/carbon vulcan XC-72R, *Biosens. Bioelectron.*, 2013, **47**, 248–257.